ELSEVIER

Contents lists available at ScienceDirect

Solid State Nuclear Magnetic Resonance

journal homepage: www.elsevier.com/locate/ssnmr





A case study on the influence of hydrophilicity on the signal enhancement by dynamic nuclear polarization

Sonja C. Döller^a, Torsten Gutmann^a, Markus Hoffmann^b, Gerd Buntkowsky^{a,*}

- a Eduard-Zintl-Institut für Anoreanische und Physikalische Chemie. Technische Universität Darmstadt. Alarich-Weiss-Str. 8. D-64287, Darmstadt. Germany
- b Department of Chemistry and Biochemistry, State University of New York College at Brockport, Brockport, NY, 14420, USA

ARTICLE INFO

Dedicated to the memory of our friend and colleague Shimon Vega 1943-2021

Keywords:
Solid state NMR
DNP NMR
Low temperature NMR
Dynamics
Surfactants
Octanol

ABSTRACT

In this work, the behavior of four different commercially available polarizing agents is investigated employing the non-ionic model surfactant 1-octanol as analyte. A relative method for the comparison of the proportion of the direct and indirect polarization transfer pathways is established, allowing a direct comparison of the polarization efficacy for different radicals and different parts of the 1-octanol molecule despite differences in radical concentration or sample amount. With this approach, it could be demonstrated that the hydrophilicity is a key factor in the way polarization is transferred from the polarizing agent to the analyte. These findings are confirmed by the determination of buildup times $T_{\rm b}$, illustrating that the choice of polarizing agent plays an essential role in ensuring an optimal polarization transfer and therefore the maximum amount of enhancement possible for DNP enhanced NMR measurements.

1. Introduction

The observation of processes that take place in living cells has been an objective of generations of molecular biologists and biochemists. Cells are complex structural units and cellular processes might not proceed the same way as when the corresponding compounds are studied in isolated form. So far, noninvasive procedures such as fluorescence based approaches [1–3], infrared (IR) spectroscopy [4], Raman spectroscopy [5] and nuclear magnetic resonance (NMR) spectroscopy are the most efficient techniques for observing dynamics and chemistry in cells. In-cell NMR spectroscopy has the advantage of being the only technique which allows studying the behavior of cellular components at atomic resolution [6] and therefore continues to be the preferred approach for finding experimental answers to a plethora of different scientific questions [6,7]. However, NMR spectroscopy suffers from its inherently low sensitivity, which is further amplified by the usually low concentrations of the biological compounds of interest as well as the observed heteronuclei, which exhibit a low gyromagnetic ratio [8–10]. Part of this issue is typically overcome with isotopic labelling [6-8], which allows to filter the desired signals against the usually suboptimal signal-to-noise-ratio caused by the biological matrix the probed molecule is located in. However, labelling a molecule with a NMR-active nucleus like ¹³C or ¹⁵N often requires elaborate synthetical efforts [11] which, depending on the location of the label, can be a tedious process. Additionally, at the low concentrations of physiologically relevant molecules, isotopic labelling alone often does not suffice to achieve adequate signal intensity.

Therefore, other specific NMR techniques that enable a sensitivity boost are of interest. Here, dynamic nuclear polarization (DNP) enhanced NMR spectroscopy has proven to be a powerful technique to enhance signals in biological systems [8,9,12,13], allowing for the observation of analytes at low concentration. In this context, dissolution DNP is typically used for investigations of biological samples since it facilitates DNP enhanced NMR experiments at room temperature and thus close to physiological conditions [8,12,14,15]. However, since the process of dissolution DNP is to a great extent irreversible due to the rapid sample dissolution in warm solvents and the polarization slowly decaying without any possibility for a de novo hyperpolarization, many biological samples continue to be investigated by DNP enhanced solid state NMR (ssNMR) at low temperatures (about 100 K). DNP enhanced ssNMR is especially the method of choice for analytes too large for fast molecular tumbling in solution, which also lack a long-range order and therefore cannot reasonably be investigated by X-ray methods [16], such as proteins [13,17-20] or structures that result of a supramolecular

E-mail address: gerd.buntkowsky@chemie.tu-darmstadt.de (G. Buntkowsky).

^{*} Corresponding author.

assembly of smaller molecules [21-23].

A polarization agent possessing unpaired electrons, such as mono or bi-radical organic compounds or high spin metal ions, need to be present in the sample for DNP enhanced NMR experiment to induce polarization transfer through cross-relaxation processes to the analyte molecules during DNP enhanced NMR experiments [14].

In recent years, the discovery of the indirect polarization transfer [24,25], which is mediated by spontaneous $^{1}\text{H}^{-13}\text{C}$ cross-relaxation within molecular groups displaying sufficient dynamics for the nuclear Overhauser effect (NOE) type effect to operate [26], has made it feasible to investigate dynamics of biological relevant systems such as amino acids [27], aptamers [28], peptides [29] and proteins [29]. Through the application of a specialized pulse sequence, the contribution of the direct and the indirect polarization transfer can be deconvoluted to yield a set of two spectra, showing only the signals caused by the direct or the indirect polarization transfer pathway, respectively [24,25,30]. This allows for the selective enhancement of the signals of mobile groups like methyl [27] and amino groups [30], or for the investigation of molecular dynamics in solids [31,32].

The location of the polarizing agent relative to the analyte molecule and the resulting intermolecular interactions with the analyte play a key role in the way the polarization is transferred to the analyte [33]. Occasionally, the polarizing agent is attached to a certain part of the analyte [34] or its environment [35], although this is not the case in most works [13]. Hence, it is fundamentally important to choose a polarization agent that is able to reach the analyte, ensuring proper interaction between the two to obtain an optimal signal enhancement [36].

In this work, four different commonly employed polarizing agents, namely AMUPol, TOTAPOL, bTbK and AsymPol (see Fig. 1), are investigated via DNP enhanced ssNMR towards their behavior in 1-octanol. 1-octanol was chosen because it serves as a membrane mimetic and provides the ideal amphiphilic properties to elucidate the polarizing agents' affinity towards different chemical environments [37,38]. $^1\mathrm{H} \rightarrow ^{13}\mathrm{C}$ CP MAS ssNMR spectra are recorded to estimate the enhancement factors for each sample. To probe the polarizing agent's location, $^{13}\mathrm{C}$ MAS DNP enhanced ssNMR measurements are performed and the direct and indirect polarization transfer pathways [25] are analyzed for the methylene carbon in proximity to the hydroxyl group, C_1 , and the methyl carbon, C_8 . Since the ratio of direct vs. indirect pathway polarization is directly influenced by the proximity of the radical to the analyte, the location of the radical in relation to the amphiphilic 1-octanol molecule

can be derived, therefore allowing the prediction of the respective polarizing agent's affinity towards certain sites of analytes in future samples. The findings of this analysis are then compared to the buildup times (T_b) of the observed carbons for each sample.

The rest of the work is organized as follows: First, the experimental section summarizes the DNP sample preparation and the applied measurement parameters utilized to record $^{13}\mathrm{C}$ CP MAS DNP NMR spectra as well as the aforementioned saturation recovery sequences at different builtup times. Subsequently, the findings of the direct νs . indirect polarization transfer pathway analysis as well as the results of the determination of the relevant buildup times T_b times are presented and discussed. The conclusions section provides a summary of the key findings and a discussion of their applicability.

2. Materials and methods

2.1. General

All chemicals were used as received. The anhydrous 1-octanol was purchased from Acros Organics and stored in a glove box under argon to prevent absorption of atmospheric water. AMUPol was purchased from CortecNet, AsymPol was donated to us by the Senker group from Bayreuth University, TOTAPOL was purchased from Dynupol and bTbK was donated to us by Ouari and coworkers from Aix-Marseille University. All radicals were stored in the freezer to prevent degradation.

2.2. Sample preparation for DNP NMR experiments

Apart from bTbK, all utilized polarizing agents were dissolved into the 1-octanol in small glass vials by manual agitation of the closed vial until all solids had dissolved and a clear solution had formed. This process usually took 10–15 min. For bTbK, the obtained suspension was shaken until no further changes in the amount of solid radical was observed. Then, the suspension was filtered through a syringe filter to remove any residual solids, obtaining a clear solution. It is estimated that about half of the solid radical was dissolved in the 1-octanol. No ultrasonication was used to prevent degradation of the polarizing agents [43]. Table 1 summarizes the utilized polarizing agents and the obtained concentrations.

The solutions were then transferred into 3.2 mm sapphire rotors using an Eppendorf pipet. The rotors were sealed with either silicon or

Fig. 1. Structures of the utilized polarizing agents AMUPol [39], TOTAPOL [40], bTbK [41] and AsymPol [42].

Table 1 Polarization agents used in this work, corresponding concentrations and obtained enhancement factors, determined from the ^{1}H \rightarrow ^{13}C CP MAS DNP experiments.

Polarizing agent	AMUPol	TOTAPOL	bTbK	AsymPol
Concentration/mM	15, 40	15	7.5*	15
Average ¹³ C enhancement	5.8, 7.5	2.4	4.11	6.4

^{*}estimated concentration of the saturated solution.

homemade rubber plugs and closed with ZrO2 driving caps.

2.3. DNP enhanced ¹³C solid state NMR spectroscopy

All ssNMR measurements were carried out on a Bruker Avance III 400 DNP NMR spectrometer operating at 9.4 T (401.63 MHz for $^1\mathrm{H},$ 100.99 MHz for $^{13}\mathrm{C}$), using a 9.7 T Bruker gyrotron system to generate microwaves (µW) at 263 GHz frequency. The spectrometer was equipped with a 3.2 mm low temperature H/X/Y triple resonance probe which was used in H/C/Y triple mode throughout all measurements. Sample temperatures were nominally 112 K and 120 K for data obtained with and without µW irradiation of the sample, respectively. A MAS rate of 8 kHz was used. Heteronuclear decoupling was performed during data acquisition using the SPINAL-64 decoupling sequence [44].

Enhancement factors for ^{13}C were calculated based on $^{1}\text{H} \rightarrow ^{13}\text{C}$ cross-polarization (CP) MAS experiments. The contact time in these experiments was set to 2 ms; a ramped pulse was applied on the $^{1}\text{H}\text{-}$ channel. Each spectrum was recorded with 16 scans. Average nominal values of the enhancement factors were obtained by scaling the peak maxima of the $\mu\text{W}\text{-}\text{off}$ spectra to those of the $\mu\text{W}\text{-}\text{on}$ spectra. These values are given in Table 1.

To determine the buildup times $T_b,$ saturation recovery experiments were employed. ^{13}C magnetization was initially quenched by applying a pulse train consisting of 20 $\pi/2$ -pulses with a respective pulse length of 3.5 μs and a delay of 5 ms between the pulses. Spectral data was acquired after buildups τ_b of 2, 4, 7.5, 16, 32, 75, 128 and 256 s, recording 128 scans for the shortest τ_b and 64 scans for all other $\tau_b.$

To be able to record the direct polarization transfer path only, the pulse sequence introduced by some of us in earlier work was applied [25]. In this sequence, the standard saturation recovery experiment was modified by the addition of a train of rotor-synchronized π -pulses with a pulse length of 6 μs on the 1H channel. The pulses were spaced 50 ms apart for all buildup times shorter than 32 s, and 500 ms apart for buildup times of 32 s and above.

The obtained spectra for the direct polarization pathway and the superposition of direct and indirect pathways were normalized to an equal number of scans and deconvoluted using Origin Pro 2021 using a Lorentzian line shape to for all signals. In this way, the intensities of the C_1 - and C_8 -signal of the 1-octanol molecule were determined and further examined, as these peaks are of interest for this work. The amount of indirect polarization was determined by subtracting the direct-pathway-only spectra from the ones obtained from the superposition of both pathways. The obtained signal intensities were plotted against the corresponding τ_b used in the experiment to determine T_b times of the carbons of interest.

3. Results and discussion

3.1. $^{1}H \rightarrow ^{13}C$ CP MAS DNP of 1-octanol

First, $^1H \rightarrow ^{13}C$ CP MAS DNP experiments were performed to determine whether signal enhancement is feasible for the four investigated radicals in 1-octanol solution and to estimate the enhancement factors. Exemplary $^1H \rightarrow ^{13}C$ CP MAS spectra of AMUPol (15 mM) dissolved in 1-octanol recorded with and without μW irradiation are shown in Fig. 2.

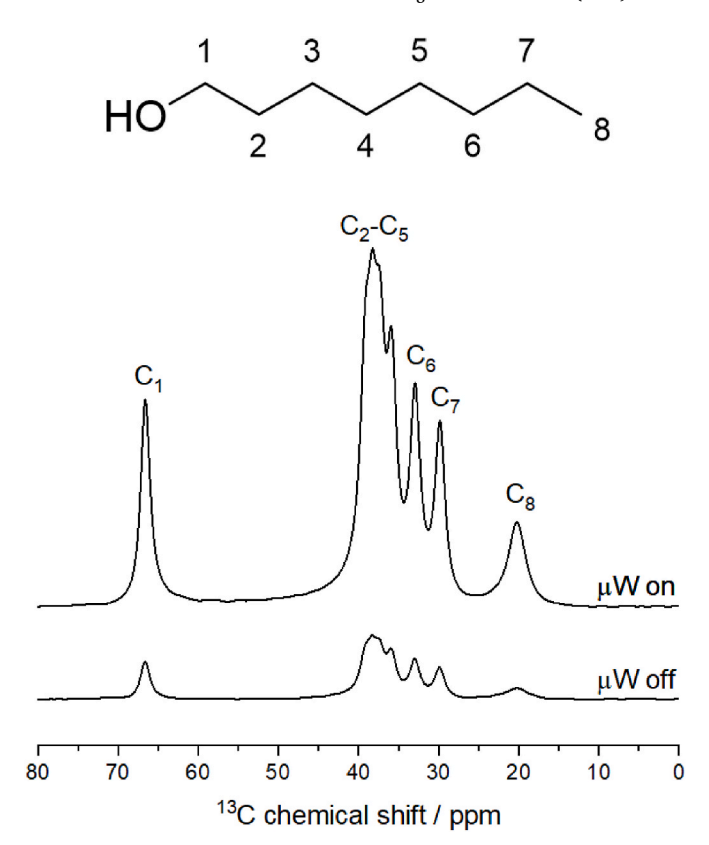


Fig. 2. $^{1}\text{H} \rightarrow ^{13}\text{C}$ CP MAS spectra recorded with μW on and μW off of AMUPol (15 mM) dissolved in 1-octanol. Also shown is the structure of 1-octanol and the corresponding peak assignments.

In the obtained spectra, the signals are assigned to the 1-octanol carbons according to their chemical surroundings. The signal at 67 ppm is attributed to C_1 , which is located closest to the hydroxyl group. The signal at 20 ppm corresponds to the methyl group of the aliphatic moiety of the 1-octanol molecule, C_8 [45]. All other signals between the C_1 and C_8 signals correspond to the methylene groups of the 1-octanol.

For comparison, the signal enhancements obtained for the various

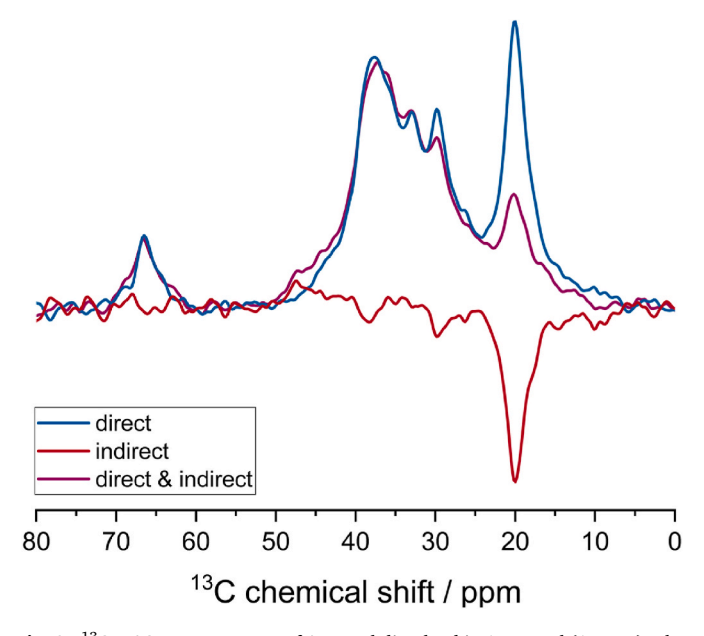


Fig. 3. ¹³C MAS DNP spectrum of AMUPol dissolved in 1-octanol (15 mM). The direct and the indirect channel as well as their superposition are displayed.

radicals in 1-octanol solution are summarized in Table 1. The largest signal enhancement ($\epsilon = 7.5$) is observed for AMUPol in 1-octanol (40 mM). Since the signal enhancement usually increases with the radical concentration until the radical concentration is high enough for the paramagnetic quenching of the polarization to prevail [46], this effect is expected. TOTAPOL shows the smallest enhancement factor ($\varepsilon = 2.4$). Due to its aliphatic linker connecting the two nitroxide radical moieties, the TOTAPOL molecule displays a relatively large degree of flexibility [46]. This hinders a more efficient polarization transfer via the Cross Effect (CE) [39], the dominant polarization transfer effect for nitroxide biradicals [33]. The more rigid radicals AMUPol, bTbK and AsymPol allow for a more efficient polarization transfer via the CE, therefore showing larger enhancement factors. The comparatively small enhancement factors documented in this work (see Table 1) are most probably caused by 1-octanol being a poor glass former, restricting efficient DNP hyperpolarization [47,48].

For all radicals, a largely homogeneous enhancement is observed for all signals. This is explained by the way in which polarization is distributed through the sample in CP experiments. The unpaired electrons of the polarizing agents are polarized by the applied μ W radiation. This polarization is transferred to the surrounding nuclei via the CE. Subsequently, the thereby created 1 H polarization spreads throughout the sample via homonuclear 1 H– 1 H spin diffusion [49]. This polarization is then transferred to the 13 C nuclei via a spinlock pulse [33,50,51].

The efficacy of the homonuclear $^{1}H^{-1}H$ spin diffusion strongly depends on the proximity of the nuclei to each other, since this process relies on dipole-dipole interactions [49]. Considering the uniform enhancement observed for all signals of 1-octanol, it is assumed that homogeneous $^{1}H^{-1}H$ spin diffusion takes place in the sample, indicating a statistically uniform distribution of $^{1}H^{-1}H$ distances in the sample. Contrary cases have been observed for analytes dissolved in either hydrophilic or hydrophobic solvent matrixes [52]. Investigations with an additional analyte and 1-octanol as solvent matrix are beyond the scope of this paper.

In the investigated case, the uniform DNP enhancement renders $^1\mathrm{H}$ \rightarrow $^{13}\mathrm{C}$ CP MAS DNP experiments unsuitable to elucidate the way the radical interacts with the analyte and its position relative to the analyte molecules.

3.2. ¹³C MAS DNP of 1-octanol – direct vs. indirect polarization transfer

DNP enhanced ¹³C MAS direct polarization experiments are applied to determine the amount of polarization that is transferred directly to the ¹³C nuclei *vs.* indirectly through the proton reservoir, allowing for a determination of the spatial proximity of the polarizing agent to certain parts of the analyte. An exemplary ¹³C MAS DNP spectrum of AMUPol dissolved in 1-octanol (15 mM) is shown in Fig. 3. The direct and the indirect channel as well as the superposition of both are illustrated.

For the methyl group observed at 20 ppm, the indirect polarization transfer pathway is consistently dominant throughout this work. The indirect polarization transfer pathway is aided by molecular motion [25], therefore the indirect polarization transfer for the rotating methyl group is significant [47]. The signal corresponding to C_7 also displays indirect polarization transfer but with less efficiency, showing that this group retains dynamics at low temperatures. All other groups only show negligible indirect polarization transfer pathway. This suggests that the 1-octanol molecules form rather rigid, supramolecular structures when frozen [47].

To allow for an elucidation of the spatial proximity of the polarizing agents to the different chemical groups of the 1-octanol molecule, the ratio of direct vs. indirect polarization transfer pathways for the carbon nuclei of interest needs to be determined. Since different samples with varying radical concentrations were investigated in this study, a comparison of the absolute signal intensities obtained by deconvoluting the spectra is not expected to yield reasonable results. Therefore, to ensure comparability between samples, a relative method to evaluate the

amount of indirect pathway polarization x_{indirect} is established in this work.

Here, the overall signal intensity is calculated as the sum of the magnitude of signal intensities $I_{\rm total}$ of the direct and indirect pathway signal ($I_{\rm direct}$ and $I_{\rm indirect}$ respectively). Subsequently, $I_{\rm indirect}$ is divided by that sum, according to eq. (1). $x_{\rm indirect}$ therefore represents the percentage of the signal intensity achieved by indirect polarization transfer compared to the total signal intensity.

$$x_{\text{indirect}} = \frac{|I_{\text{indirect}}|}{I_{\text{direct}} + |I_{\text{indirect}}|} = \frac{|I_{\text{indirect}}|}{I_{\text{total}}}$$
(1)

Since the value $x_{\rm indirect}$ only depends on the ratio of two signal intensities obtained from the same sample, parameters such as the sample amount or the amount of radical used are removed by the division. Therefore, this approach can be used to compare the dependency of the ratio of the direct vs. the indirect polarization pathway for different radicals.

3.3. Analysis of the ratios of direct vs. indirect polarization for different radicals

The analysis of the ratios of direct νs . indirect polarization transfer pathways for each radical, buildup time τ_b and carbon of interest is illustrated in Fig. 4. This is done by plotting $x_{indirect}$ as a function of τ_b of the experiment for each radical and for both C_1 and C_8 of the 1-octanol molecule.

Fig. 4a shows x_{indirect} for the methyl carbon of the 1-octanol molecule for the hydrophilic radicals AMUPol and TOTAPOL as a function of τ_h . The polarization builds up very quickly for both radicals, showing that the indirect polarization transfer pathway is highly efficient throughout the entire span of τ_b . Comparing the polarization transfer patterns for different concentrations of AMUPol, an overall slight decrease of the efficiency of indirect polarization transfer is observed with increased concentration. This confirms that the addition of more polarizing agent and therefore the statistic increase of spatial proximity lowers the amount of indirect pathway polarization. This effect is in accordance with what was observed by some of the authors earlier [25]. The AMUPol samples show the most efficient polarization transfer via the indirect pathway for the methyl group, illustrating a less efficient polarization transfer via the direct pathway in return. This suggests a large distance between the aliphatic moiety of the 1-octanol molecule and the polarizing agent, inhibiting an efficient direct transfer of polarization from the radical to the C8. It also demonstrates the high amount of dynamics the methyl group retains at low temperatures [27].

In Fig. 4b, the analysis is shown for the methylene carbon neighboring the hydroxyl group of the 1-octanol molecule. For both AMUPol and TOTAPOL, the indirect polarization builds up very quickly, reaching a maximum after 4 s and decaying afterwards as the direct polarization transfer pathway becomes the dominant one. Apparently, the indirect polarization transfer pathway through the proton reservoir proceeds faster than the direct polarization transfer from the radical to the C₁ via the CE. This effect is observable despite the suggested closer proximity of the hydrophilic radical to the C₁. In this work, protonated 1-octanol as well as a constant μW -source have been used. The relatively uniform enhancement throughout the 1-octanol molecule observed for the $^{1}H \rightarrow$ ¹³C CP MAS DNP experiments show that hyperpolarization spreads through the proton reservoir evenly. This means that it's highly likely that the proton reservoir surrounding the carbon atoms has been hyperpolarized long before the actual measurements take place. Considering the relatively small concentrations of the utilized polarizing agents, it is statistically more likely for any carbon to be polarized via the hyperpolarized proton reservoir. Therefore, the indirect pathway polarization is quicker to hyperpolarize the observed carbon atoms not directly neighboring the polarization agent before dissipating throughout the 1-octanol in the case of longer τ_b .

For both AMUPol concentrations, a much smaller percentage of

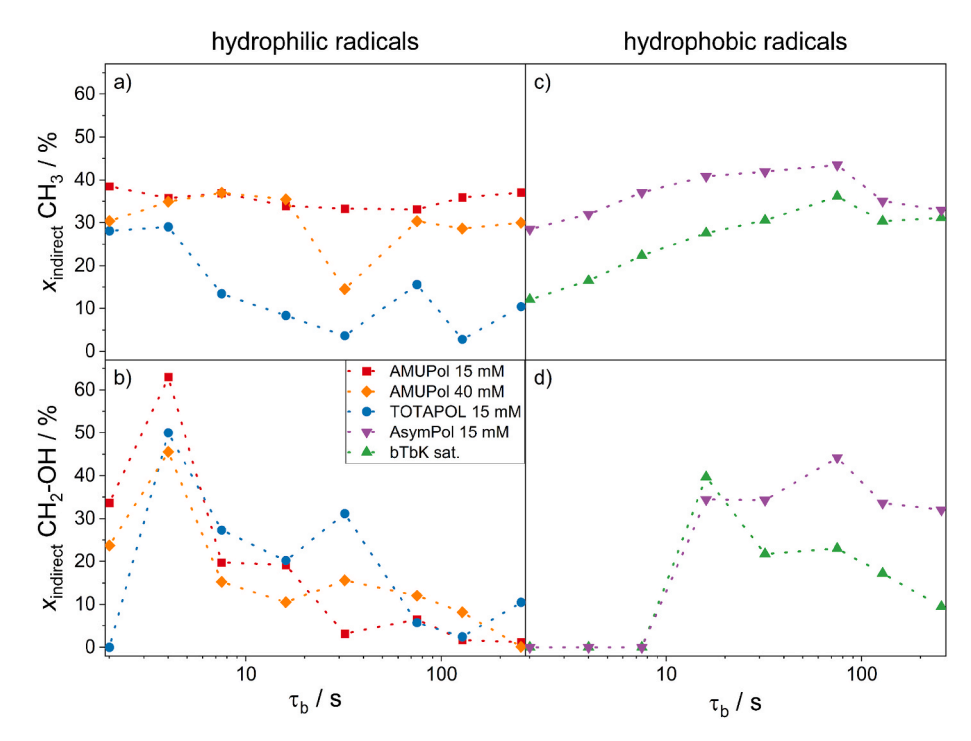


Fig. 4. Ratios of indirect polarization compared to the total signal intensity for the methyl group (panel a and c) and the methylene group neighboring the hydroxyl group of the 1-octanol molecule (panel b and d) as a function of τ_b . The hydrophilic and hydrophobic radicals are displayed separately to facilitate interpretation.

indirect polarization transfer is observed at long τ_b compared to the methyl carbon, pointing to a close spatial proximity of the AMUPol radical to the C_1 . Considering that AMUPol is a highly hydrophilic polarizing agent [39], it is to be expected to be found close to the hydroxyl group of the 1-octanol molecule, which explains the presented findings. Additionally, the methylene group is less mobile than the methyl group at the present temperatures [53], generally lowering its affinity towards the indirect polarization transfer pathway.

TOTAPOL shows a generally low affinity for the indirect polarization pathway for both investigated carbons (Fig. 4a and b). TOTAPOL is the most flexible of the investigated polarizing agents (see Fig. 1 for structures of utilized polarizing agents) [40,41,46], which would usually lead to the analyte molecules not being able to approach the radical as closely as possible for more rigid radicals. This would lead to an increase of the observed indirect channel polarization transfer [31]. A possible reason for this behavior might be due to the inherent dynamics of the polarizing agent disturbing the local supramolecular structure formed by the 1-octanol molecules, preventing the analyte molecule from forming the usually observed micelles or ribbons [54–56]. Hence, a more glass-like phase of 1-octanol might form around the TOTAPOL molecules, facilitating the direct polarization transfer and leading to the polarizing agent being distributed more evenly in the relevant part of the solution.

Fig. 4c shows the ratios of the indirect polarization pathway for the methyl group and the hydrophobic radicals, AsymPol and bTbK. Both polarizing agents show comparable ratios of the direct vs. the indirect polarization transfer pathway and a slow increase of the amount of the indirect pathway polarization until a maximum is reached and the indirect polarization transfer pathway becomes less pronounced for long buildup times ($\tau_b \geq 128\,$ s). bTbK shows less indirect polarization transfer than AsymPol initially. This finding suggests a proximity of the bTbK molecules to the C_8 , aiding a direct polarization transfer, which is in agreement to bTbK being the most hydrophobic and therefore most lipophilic polarizing agent investigated in this work [41].

The methylene group neighboring the hydroxyl group generally shows a slow buildup when the hydrophobic radicals are utilized (Fig. 4d). This points to an ineffective polarization transfer to the $\rm C_1$ and therefore a large distance between the radicals and the methylene group.

It is assumed that the methylene group takes part in the formation of supramolecular structures and therefore is generally less accessible for surrounding molecules [53,57], therefore impeding polarization transfer of any kind. When a hydrophilic polarizing agent is employed, it is probably able to insert itself somewhere close to the C_1 in this supramolecular structure, aiding the polarization transfer. In contrast to that, the investigated hydrophobic polarizing agents are not able to disturb the formation of supramolecular structures at the hydrophilic moiety of the 1-octanol molecule.

After a buildup time of 16 s, the first signal of the C_1 can be observed, which then displays a large amount of indirect polarization transfer. Interestingly, the amount of indirect polarization transfer reduces for bTbK with longer τ_b , again suggesting that the direct polarization transfer pathway becomes more dominant the longer the experimental τ_b is. As the buildup of the indirect polarization seems to be quicker than the one of the direct polarization, it is possible that the decay is caused by the indirect polarization reaching the C_1 and potentially dissipating throughout the 1-octanol molecule before the actual spectrum is measured.

Interestingly, AsymPol does not show the same decay of the indirect polarization as it remains at a relatively constant level after the initial buildup. As AsymPol was computationally devised to have a large electron dipolar coupling between its two radical moieties, its defining feature is a very short polarization buildup time [42]. This short buildup time might lead to a constant repolarization of the proton reservoir, which then repolarizes the investigated C_1 throughout the applied τ_b , therefore leading to a constant amount of indirect polarization reaching the $C_1.$

3.4. Investigation of C_1 and C_8 buildup times

To confirm the findings of the previous analysis, the direct buildup times of the investigated carbons were determined under the influence of the different radicals. Direct polarization transfer can only proceed when the observed carbon is in the vicinity of the radical since natural abundance homonuclear $^{13}\mathrm{C}$ spin diffusion is inefficient [25]. Hence, the length of the direct T_b time of a certain carbon atom in the 1-octanol

molecule can be used to estimate its proximity to the polarizing agents. Fig. 5 shows the determined direct T_b times for both the methylene carbon C_1 and the methyl carbon C_8 . The corresponding buildup curves can be found in Fig. S1 in the Supporting Informations.

The methyl group shows a much quicker buildup than the methylene group for all utilized polarizing agents, a phenomenon which is well-documented and understood to be due to the rotor motions of methyl end groups that remain active even at very low temperatures [14,19,27, 31].

AMUPol in 1-octanol (15 mM), the most hydrophilic radical used in this work [39], shows the longest T_b time at the C_8 and the shortest T_b time at the C_1 , indicating a spatial proximity of the AMUPol to the hydrophilic end of the molecule. Increasing the concentration of the AMUPol to 40 mM and therefore increasing the average proximity of the polarizing agent to the 1-octanol leads to a slight decrease of the T_b times for the methylene carbon. Since an increased concentration of the radical aids in the polarization transfer, this observation is expected [33]. However, an increased concentration of AMUPol does not lead to a significant decrease of the T_b time for the methyl carbon. It is therefore assumed that the AMUPol molecules strongly favor an orientation towards the hydroxyl group of the 1-octanol, despite the heightened concentration.

BTbK and AsymPol, the hydrophobic polarizing agents investigated in this study [41,42], show significantly shorter T_b times for the C_8 compared to the much longer T_b times for the C_1 , demonstrating that the radicals are preferably located towards the aliphatic moiety of the 1-octanol molecule.

TOTAPOL, which is expected to behave similarly to AMUPol since it also falls in the range of hydrophilic polarizing agents, shows T_b times which lie closer to those of the hydrophobic radicals. Due to its dynamics within the linker connecting the two radical moieties and therefore less efficient overall polarization transfer [41], longer Tb times were expected for TOTAPOL at all positions of the 1-octanol molecule. For C₁, this expectation has been confirmed as a long $T_{\mbox{\scriptsize b}}$ time is observed for this carbon despite the assumption that the hydrophilic TOTAPOL might have an affinity for the position close to the hydrophilic moiety of the 1-octanol. However, for C₈, a shorter T_b time is observed compared to the other hydrophilic radicals. Considering that the observed T_b times for TOTAPOL are not matching the ones observed for AMUPol, a rigid hydrophilic biradical, the hypothesis of TOTAPOL's dynamic disturbing the local structure of the analyte 1-octanol and therefore leading to a more glass-like 1-octanol phase with statistically distributed TOTAPOL molecules might explain the unexpected behavior of the Tb times observed for TOTAPOL.

4. Conclusion

DNP enhanced ssNMR of different radicals dissolved in the amphiphilic 1-octanol was utilized to illustrate the influence of the choice of polarizing agent and its properties on the observed polarization transfer pathways. The polarizing agents AMUPol, bTbK, AsymPol and TOTA-POL were investigated in this work. To achieve comparable results across all samples, independent of radical concentration and amount of sample used, a relative method was established to quantify the proportion of indirectly transferred polarization expressed as a percentage of the total signal intensity. Using this method, it could be shown that the hydrophilicity of the polarizing agents plays a key role in which part of the 1-octanol molecule is polarized via which polarization pathway. AMUPol, a hydrophilic polarizing agent, preferably polarizes the hydrophilic moiety of the 1-octanol directly, while bTbk, a hydrophobic polarizing agent, shows a stronger affinity towards directly polarizing the aliphatic part of the 1-octanol. Interestingly, TOTAPOL does not seem to favor the indirect polarization pathway for either of the investigated carbons. This observation is explained with the relatively low rigidity of the TOTAPOL-molecule which allows a high degree of dynamics, therefore disturbing the otherwise rigid supramolecular

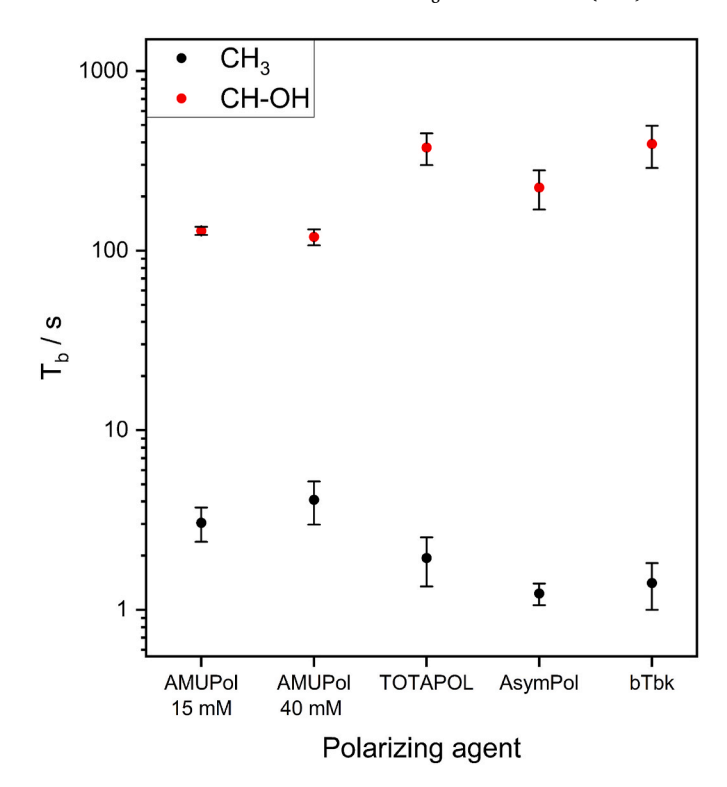


Fig. 5. Determined direct T_b values for the methyl carbon C_8 and the relevant methylene carbon C_1 .

organization of the amphiphilic 1-octanol molecules and facilitating the direct polarization transfer in a glass-like 1-octanol phase around the TOTAPOL molecules.

To confirm these findings, T_b times of the carbons of interests were determined via the recorded saturation recovery experiments. For the hydrophobic polarizing agents and the methyl carbon of the 1-octanol molecule, short T_b times were observed, indicating a very quick buildup of polarization, suggesting a close proximity of these carbon atoms to the radical. For the methylene group neighboring the hydroxyl group, long T_b times are observed for the hydrophobic polarizing agents. The hydrophilic polarizing agents are shown to lead to shorter T_b times for the methylene group of interest, lowering the time constant by their affinity to the hydroxyl group. For the methyl carbon, longer T_b times are observed compared to the lipophilic polarization agents. Again, TOTAPOL does not follow any trend that might be assumed from its hydrophilic nature, constituting an exception to the trends observed in this study.

The findings presented in this work lay the foundation of enabling informed radical choices for specific samples. Especially in biological samples like cellular components, which consist of large molecules or molecules that are part of supramolecular structures, the presented findings enable researchers to make informed choices of polarizing agent targeting optimum polarization of the nuclei of interest.

Declaration of competing interest

The authors declare that they have no known competing financial interests or personal relationships that could have appeared to influence the work reported in this paper.

Data availability

Data is available in the supplementary information.

Acknowledgements

Financial support by the Deutsche Forschungsgemeinschaft under Contract Bu-911-24-2 and by the National Science Foundation under Grant No. 1953428 are gratefully acknowledged. The authors would also like to thank Prof. Senker and coworkers from Bayreuth University and Dr. Ouari and coworkers from Aix-Marseille University for gifting us the utilized AsymPol and bTbK, respectively.

Appendix A. Supplementary data

Supplementary data to this article can be found online at https://doi.org/10.1016/j.ssnmr.2022.101829.

References

- R. Henriques, C. Griffiths, E. Hesper Rego, M.M. Mhlanga, PALM and STORM: unlocking live-cell super-resolution, Biopolymers 95 (2011) 322–331, https://doi. org/10.1002/bip.21586.
- [2] L. Stryer, Fluorescence energy transfer as a spectroscopic ruler, Annu. Rev. Biochem. 47 (1978) 819–846, https://doi.org/10.1146/annurev. bi 47 070178 004131
- [3] P. Trigo-Mourino, T. Thestrup, O. Griesbeck, C. Griesinger, S. Becker, Dynamic tuning of FRET in a green fluorescent protein biosensor, Sci. Adv. 5 (2019), eaaw4988, https://doi.org/10.1126/sciadv.aaw4988.
- [4] Y. Wang, W. Dai, Z. Liu, J. Liu, J. Cheng, Y. Li, X. Li, J. Hu, J. Lü, Single-cell infrared microspectroscopy quantifies dynamic heterogeneity of mesenchymal stem cells during adipogenic differentiation, Anal. Chem. 93 (2021) 671–676, https://doi.org/10.1021/acs.analchem.0c04110.
- [5] R. Smith, K.L. Wright, L. Ashton, Raman spectroscopy: an evolving technique for live cell studies, Analyst 141 (2016) 3590–3600, https://doi.org/10.1039/ C6AN00152A.
- [6] D.I. Freedberg, P. Selenko, Live cell NMR, Annu. Rev. Biophys. 43 (2014) 171–192, https://doi.org/10.1146/annurev-biophys-051013-023136.
- [7] T. Ikeya, P. Güntert, Y. Ito, Protein structure determination in living cells, Int. J. Mol. Sci. 20 (2019), https://doi.org/10.3390/ijms20102442.
- [8] S. Meier, M. Karlsson, P.R. Jensen, M.H. Lerche, J.Ø. Duus, Metabolic pathway visualization in living yeast by DNP-NMR, Mol. Biosyst. 7 (2011) 2834–2836, https://doi.org/10.1039/c1mb05202k.
- [9] H. Takahashi, I. Ayala, M. Bardet, G. de Paëpe, J.-P. Simorre, S. Hediger, Solid-state NMR on bacterial cells: selective cell wall signal enhancement and resolution improvement using dynamic nuclear polarization, J. Am. Chem. Soc. 135 (2013) 5105–5110, https://doi.org/10.1021/ja312501d.
- [10] J.-H. Ardenkjaer-Larsen, G.S. Boebinger, A. Comment, S. Duckett, A.S. Edison, F. Engelke, C. Griesinger, R.G. Griffin, C. Hilty, H. Maeda, G. Parigi, T. Prisner, E. Ravera, J. van Bentum, S. Vega, A. Webb, C. Luchinat, H. Schwalbe, L. Frydman, Facing and overcoming sensitivity challenges in biomolecular NMR spectroscopy, Angew. Chem. Int. Ed. 54 (2015) 9162–9185, https://doi.org/10.1002/anie.201410653.
- [11] A. Pardi, Isotope labelling for NMR studies of biomolecules, Curr. Opin. Struct. Biol. 2 (1992) 832–835, https://doi.org/10.1016/0959-440X(92)90107-I.
- [12] M.H. Lerche, P.R. Jensen, M. Karlsson, S. Meier, NMR insights into the inner workings of living cells, Anal. Chem. 87 (2015) 119–132, https://doi.org/10.1021/ ac501467x.
- [13] Ü. Akbey, H. Oschkinat, Structural biology applications of solid state MAS DNP NMR, J. Magnet. Resonance (San Diego, Calif) 269 (2016) (1997) 213–224, https://doi.org/10.1016/j.jmr.2016.04.003.
- [14] T. Biedenbänder, V. Aladin, S. Saeidpour, B. Corzilius, Dynamic nuclear polarization for sensitivity enhancement in biomolecular solid-state NMR, Chem. Rev. 122 (2022) 9738–9794, https://doi.org/10.1021/acs.chemrev.1c00776.
- [15] J.H. Ardenkjaer-Larsen, B. Fridlund, A. Gram, G. Hansson, L. Hansson, M. H. Lerche, R. Servin, M. Thaning, K. Golman, Increase in signal-to-noise ratio of 10,000 times in liquid-state NMR, Proc. Natl. Acad. Sci. U.S.A. 100 (2003) 10158–10163, https://doi.org/10.1073/pnas.1733835100.
- [16] A.Y. Fadeev, T.J. McCarthy, Trialkylsilane monolayers covalently attached to silicon surfaces: wettability studies indicating that molecular topography contributes to contact angle hysteresis, Langmuir 15 (1999) 3759–3766, https:// doi.org/10.1021/la9814860.
- [17] M. Hong, W.F. DeGrado, Structural basis for proton conduction and inhibition by the influenza M2 protein, Protein Sci. 21 (2012) 1620–1633, https://doi.org/ 10.1002/pro.2158
- [18] V.S. Mandala, J.K. Williams, M. Hong, Structure and dynamics of membrane proteins from solid-state NMR, Annu. Rev. Biophys. 47 (2018) 201–222, https://doi.org/10.1146/annurev-biophys-070816-033712.
- [19] J. Mao, V. Aladin, X. Jin, A.J. Leeder, L.J. Brown, R.C.D. Brown, X. He, B. Corzilius, C. Glaubitz, Exploring protein structures by DNP-enhanced methyl solid-state NMR spectroscopy, J. Am. Chem. Soc. 141 (2019) 19888–19901, https://doi.org/ 10.1021/jacs.9b11195.
- [20] E. Nimerovsky, K.T. Movellan, X.C. Zhang, M.C. Forster, E. Najbauer, K. Xue, R. Dervişoğlu, K. Giller, C. Griesinger, S. Becker, L.B. Andreas, Proton detected

- solid-state NMR of membrane proteins at 28 tesla (1.2 GHz) and 100 kHz magic-angle spinning, Biomolecules 11 (2021), https://doi.org/10.3390/biom11050752.
- [21] A.K. Schütz, Solid-state NMR approaches to investigate large enzymes in complex with substrates and inhibitors, Biochem. Soc. Trans. 49 (2021) 131–144, https:// doi.org/10.1042/BST20200099.
- [22] M. Weingarth, M. Baldus, Solid-state NMR-based approaches for supramolecular structure elucidation, Acc. Chem. Res. 46 (2013) 2037–2046, https://doi.org/ 10.1021/ar300316e
- [23] S. Yan, C.L. Suiter, G. Hou, H. Zhang, T. Polenova, Probing structure and dynamics of protein assemblies by magic angle spinning NMR spectroscopy, Acc. Chem. Res. 46 (2013) 2047–2058, https://doi.org/10.1021/ar300309s.
- [24] D. Daube, V. Aladin, J. Heiliger, J.J. Wittmann, D. Barthelmes, C. Bengs, H. Schwalbe, B. Corzilius, Heteronuclear cross-relaxation under solid-state dynamic nuclear polarization, J. Am. Chem. Soc. 138 (2016) 16572–16575, https://doi.org/10.1021/jacs.6b08683.
- [25] M.M. Hoffmann, S. Bothe, T. Gutmann, F.-F. Hartmann, M. Reggelin, G. Buntkowsky, Directly vs indirectly enhanced 13 C in dynamic nuclear polarization magic angle spinning NMR experiments of nonionic surfactant systems, J. Phys. Chem. C 121 (2017) 2418–2427, https://doi.org/10.1021/acs. ipcc.6b13087.
- [26] A.W. Overhauser, Polarization of nuclei in metals, Phys. Rev. 92 (1953) 411–415, https://doi.org/10.1103/PhysRev.92.411.
- [27] V. Aladin, B. Corzilius, Methyl dynamics in amino acids modulate heteronuclear cross relaxation in the solid state under MAS DNP, Solid State Nucl. Magn. Reson. 99 (2019) 27–35, https://doi.org/10.1016/j.ssnmr.2019.02.004.
- [28] V. Aladin, M. Vogel, R. Binder, I. Burghardt, B. Suess, B. Corzilius, Complex formation of the tetracycline-binding aptamer investigated by specific crossrelaxation under DNP, Angew. Chem. Int. Ed. 58 (2019) 4863–4868, https://doi. org/10.1002/anie.201811941.
- [29] Q.Z. Ni, E. Markhasin, T.V. Can, B. Corzilius, K.O. Tan, A.B. Barnes, E. Daviso, Y. Su, J. Herzfeld, R.G. Griffin, Peptide and protein dynamics and low-temperature/DNP magic angle spinning NMR, J. Phys. Chem. B 121 (2017) 4997–5006. https://doi.org/10.1021/acs.jpcb.7b02066.
- [30] H. Park, B. Uluca-Yazgi, S. Heumann, R. Schlögl, J. Granwehr, H. Heise, P.P. M. Schleker, Heteronuclear cross-relaxation effect modulated by the dynamics of N-functional groups in the solid state under 15N DP-MAS DNP, J. Magn. Reson. 312 (2020), 106688, https://doi.org/10.1016/j.jmr.2020.106688.
- [31] M.M. Hoffmann, S. Bothe, T. Gutmann, G. Buntkowsky, Unusual local molecular motions in the solid state detected by dynamic nuclear polarization enhanced NMR spectroscopy, J. Phys. Chem. C 121 (2017) 22948–22957, https://doi.org/ 10.1021/acs.incc.7b07965.
- [32] M.M. Hoffmann, S. Bothe, M. Brodrecht, V. Klimavicius, N.B. Haro-Mares, T. Gutmann, G. Buntkowsky, Direct and indirect dynamic nuclear polarization transfer observed in mesoporous materials impregnated with nonionic surfactant solutions of polar polarizing agents, J. Phys. Chem. C 124 (2020) 5145–5156, https://doi.org/10.1021/acs.jpcc.9910504.
- [33] A.S. Lilly Thankamony, J.J. Wittmann, M. Kaushik, B. Corzilius, Dynamic nuclear polarization for sensitivity enhancement in modern solid-state NMR, Prog. Nucl. Magn. Reson. Spectrosc. 102–103 (2017) 120–195, https://doi.org/10.1016/j. pnmrs.2017.06.002.
- [34] J. Heiliger, T. Matzel, E.C. Çetiner, H. Schwalbe, G. Kuenze, B. Corzilius, Site-specific dynamic nuclear polarization in a Gd(III)-labeled protein, Phys. Chem. Chem. Phys. 22 (2020) 25455–25466. https://doi.org/10.1039/d0cp05021k.
- [35] M. Juramy, R. Chevre, P. Cerreia Vioglio, F. Ziarelli, E. Besson, S. Gastaldi, S. Viel, P. Thureau, K.D.M. Harris, G. Mollica, Monitoring crystallization processes in confined porous materials by dynamic nuclear polarization solid-state nuclear magnetic resonance, J. Am. Chem. Soc. 143 (2021) 6095–6103, https://doi.org/ 10.1021/jacs.0c12982.
- [36] S.Y. Liao, M. Lee, T. Wang, I.V. Sergeyev, M. Hong, Efficient DNP NMR of membrane proteins: sample preparation protocols, sensitivity, and radical location, J. Biomol. NMR 64 (2016) 223–237, https://doi.org/10.1007/s10858-016-0023-3.
- [37] C.A.F. de Oliveira, C.R.W. Guimares, R.B. de Alencastro, Molecular dynamics study on liquid 1-octanol, Int. J. Quant. Chem. 80 (2000) 999–1006, https://doi.org/ 10.1002/1097-461X(2000)80:4/5<999:AID-QUA48>3.0.CO;2-K.
- [38] P. Sassi, M. Paolantoni, R.S. Cataliotti, F. Palombo, A. Morresi, Water/alcohol mixtures: a spectroscopic study of the water-saturated 1-octanol solution, J. Phys. Chem. B 108 (2004) 19557–19565, https://doi.org/10.1021/jp046647d.
- [39] C. Sauvée, M. Rosay, G. Casano, F. Aussenac, R.T. Weber, O. Ouari, P. Tordo, Highly efficient, water-soluble polarizing agents for dynamic nuclear polarization at high frequency, Angew. Chem. 52 (2013) 10858–10861, https://doi.org/ 10.1002/cnip.3204657.
- [40] C. Song, K.-N. Hu, C.-G. Joo, T.M. Swager, R.G. Griffin, TOTAPOL: a biradical polarizing agent for dynamic nuclear polarization experiments in aqueous media, J. Am. Chem. Soc. 128 (2006) 11385–11390, https://doi.org/10.1021/ja061284b.
- [41] Y. Matsuki, T. Maly, O. Ouari, H. Karoui, F. Le Moigne, E. Rizzato, S. Lyubenova, J. Herzfeld, T. Prisner, P. Tordo, R.G. Griffin, Dynamic nuclear polarization with a rigid biradical, Angew. Chem. 48 (2009) 4996–5000, https://doi.org/10.1002/ anie.200805940.
- [42] F. Mentink-Vigier, I. Marin-Montesinos, A.P. Jagtap, T. Halbritter, J. van Tol, S. Hediger, D. Lee, S.T. Sigurdsson, G. de Paëpe, Computationally assisted design of polarizing agents for dynamic nuclear polarization enhanced NMR: the AsymPol family, J. Am. Chem. Soc. 140 (2018) 11013–11019, https://doi.org/10.1021/ iacs.8b04911.
- [43] L.J. Kirschenbaum, P. Riesz, Sonochemical degradation of cyclic nitroxides in aqueous solution, Ultrason. Sonochem. 19 (2012) 1114–1119, https://doi.org/ 10.1016/j.ultsonch.2012.01.014.

- [44] B.M. Fung, A.K. Khitrin, K. Ermolaev, An improved broadband decoupling sequence for liquid crystals and solids, J. Magn. Reson. 142 (2000) 97–101, https://doi.org/10.1006/jmre.1999.1896.
- [45] AIST, Spectral Database for Organic Compounds, vol. 1, Octanol, 1999. https://sdbs.db.aist.go.jp/. (Accessed 17 May 2022).
- [46] K.-N. Hu, C. Song, H.-H. Yu, T.M. Swager, R.G. Griffin, High-frequency dynamic nuclear polarization using biradicals: a multifrequency EPR lineshape analysis, J. Chem. Phys. 128 (2008), 52302, https://doi.org/10.1063/1.2816783.
- [47] S.C. Döller, M. Brodrecht, N.B. Haro Mares, H. Breitzke, T. Gutmann, M. Hoffmann, G. Buntkowsky, Deuterium NMR studies of the solid–liquid phase transition of octanol- d17 confined in SBA-15, J. Phys. Chem. C 125 (2021) 25155–25164, https://doi.org/10.1021/acs.jpcc.1c05873.
- [48] F. Mentink-Vigier, Ü. Akbey, H. Oschkinat, S. Vega, A. Feintuch, Theoretical aspects of magic angle spinning - dynamic nuclear polarization, J. Magn. Reson. 258 (2015) 102–120, https://doi.org/10.1016/j.jmr.2015.07.001.
- [49] A.B. Barnes, G. de Paëpe, P.C.A. van der Wel, K.-N. Hu, C.-G. Joo, V.S. Bajaj, M. L. Mak-Jurkauskas, J.R. Sirigiri, J. Herzfeld, R.J. Temkin, R.G. Griffin, High-field dynamic nuclear polarization for solid and solution biological NMR, Appl. Magn. Reson. 34 (2008) 237–263, https://doi.org/10.1007/s00723-008-0129-1.
- [50] A. Pines, M.G. Gibby, J.S. Waugh, Proton-enhanced nuclear induction spectroscopy. A method for high resolution NMR of dilute spins in solids, J. Chem. Phys. 56 (1972) 1776–1777, https://doi.org/10.1063/1.1677439.

- [51] Y. Hovav, A. Feintuch, S. Vega, Theoretical aspects of Dynamic Nuclear Polarization in the solid state - the cross effect, J. Magn. Reson. 214 (2012) 29–41, https://doi.org/10.1016/j.jmr.2011.09.047.
- [52] T. Gutmann, B. Kumari, L. Zhao, H. Breitzke, S. Schöttner, C. Rüttiger, M. Gallei, Dynamic nuclear polarization signal amplification as a sensitive probe for specific functionalization of complex paper substrates, J. Phys. Chem. C 121 (2017) 3896–3903, https://doi.org/10.1021/acs.jpcc.6b11751.
- [53] G. Buntkowsky, S. Döller, N. Haro-Mares, T. Gutmann, M. Hoffmann, Solid-state NMR studies of non-ionic surfactants confined in mesoporous silica, Z. Phys. Chem. 236 (2022) 939–960, https://doi.org/10.1515/zpch-2021-3132.
- [54] K. Hu, Y. Zhou, J. Shen, Z. Ji, G. Cheng, Microheterogeneous structure of 1-octanol in neat and water-saturated state, J. Phys. Chem. B 111 (2007) 10160–10165, https://doi.org/10.1021/jp072847o.
- [55] N.P. Franks, M.H. Abraham, W.R. Lieb, Molecular organization of liquid n-octanol: an X-ray diffraction analysis, J. Pharmacol. Sci. 82 (1993) 466–470, https://doi. org/10.1002/jps.2600820507.
- [56] H.A. Shallard-Brown, D.J. Watkin, A.R. Cowley, n-Octanol, Acta Crystallogr. 61 (2005) o213–o214, https://doi.org/10.1107/S1600536804032775.
- [57] B. Kumari, M. Brodrecht, H. Breitzke, M. Werner, B. Grünberg, H.-H. Limbach, S. Forg, E.P. Sanjon, B. Drossel, T. Gutmann, G. Buntkowsky, Mixtures of alcohols and water confined in mesoporous silica: a combined solid-state NMR and molecular dynamics simulation study, J. Phys. Chem. C 122 (2018) 19540–19550, https://doi.org/10.1021/acs.jpcc.8b04745.